Tools for genetic manipulation of the endemic fungal pathogen, *Emergomyces africanus,* and the application of a fluorescent reporter strain in infection models

Lucian Duvenage[1,2,3]# , Alisha Chetty[1,2,3], Darren D. Thomson[4], Elizabeth R. Ballou[4], Nelesh P. Govender[5,6], Chad A. Rappleye[7]*, J. Claire Hoving[1,2,3]*

1. CMM AFRICA Medical Mycology Research Unit, Institute of Infectious Disease and Molecular Medicine, Faculty of Health Sciences, University of Cape Town, Cape Town, South Africa
2. Wellcome Centre for Infectious Diseases Research in Africa, Institute of Infectious Diseases and Molecular Medicine, University of Cape Town, Cape Town, South Africa
3. Division of Immunology, Department of Pathology, Faculty of Health Sciences, University of Cape Town, Cape Town, South Africa
4. MRC Centre for Medical Mycology, The University of Exeter, Exeter, United Kingdom.
5. Wits Mycology Division, School of Pathology, Faculty of Health Sciences, University of the Witwatersrand, Parktown, Gauteng, South Africa.
6. National Institute for Communicable Diseases, A Division of the National Health Laboratory Service, Johannesburg, Gauteng, South Africa
7. Department of Microbiology, Ohio State University, Columbus, OH, USA

*(CAR and JCH are co-senior authors)

Address correspondence to: Lucian Duvenage, lucian.duvenage@uct.ac.za

Running title: Molecular tools for Emergomyces africanus

Abstract

Emergomyces africanus is a thermally dimorphic fungal pathogen endemic to Southern Africa, which can cause fatal systemic infections in persons with advanced HIV disease. Its mechanisms of pathogenesis are not well understood. Characterisation of virulence traits in this pathogen requires appropriate molecular tools for genetic manipulation. Molecular technologies developed for the transformation of *H. capsulatum* were adapted for use in *E. africanus. Agrobacterium*-mediated transformation was used to generate a reporter strain expressing green fluorescent protein (GFP). The *E. africanus* GFP reporter strain facilitated the study of yeast interaction with macrophages *in vitro* and allowed the identification of infected phagocyte cell types in the mouse lung by flow cytometry. *E. africanus* could also maintain episomal plasmids with telomere-like sequences to introduce expression constructs without genome modification. Using this plasmid system, RNA interference constructs were used to knock down the expression of cell wall α(1,3)-glucan by targeting the transcripts of the α-glucan synthase (*AGS1*). An episomal CRISPR/Cas9 system was evaluated for *E. africanus*, which effectively disrupted *GFP* in a reporter strain and enabled the generation of a *URA5* uracil auxotroph. These tools and strains will facilitate future studies to elucidate the mechanisms of pathogenesis of *E. africanus.*

Importance

Emergomyces africanus is an opportunistic fungal pathogen affecting persons with advanced HIV disease in South Africa. The biology and pathogenesis of *E. africanus*

are not well understood, as the importance of the disease caused by this fungus (emergomycosis) has only been recognised in recent years, and molecular studies have been impaired by the lack of genetic technologies. In this work, we describe tools and methods for the genetic modification of this pathogen, which will accelerate future studies investigating how the fungus causes disease in the human host. These essential tools include (1) the ability to create fluorescent reporter strains, such as the green fluorescent protein *E. africanus* strain described here, which facilitates tracking the spread of the fungus during infection and enhances microscopy studies, (2) methods for knocking down gene expression in *E. africanus*, and (3) the permanent disruption of genes through CRISPR/Cas9 gene editing.

Introduction

Emergomyces africanus, part of the recently classified genus *Emergomyces* (1), is a fungal pathogen of humans endemic to Southern Africa (2). The fungus can cause life-threatening systemic infection in immunocompromised individuals, which, in South Africa, has exclusively been persons with advanced HIV disease (3). Because this pathogen is less often suspected by clinicians, patients affected by emergomycosis often are diagnosed only at the late stages of infection, characterised by widespread skin lesions. An understanding of its biology and host-pathogen interaction is needed to develop effective diagnostics and treatment strategies for this infection in high-risk populations.

E. africanus is a thermally dimorphic fungus. It exists in a saprobic mycelial phase in soil and releases airborne conidia (4), which, when inhaled by the host, transition to a yeast phase triggered by body temperature (5). The mechanisms by which these yeast

85 cells infect host cells are unknown. The ability to genetically manipulate a fungal
86 pathogen can open new avenues of research, whether by examining the effects of
87 gene deletions or introducing reporter genes for a wide range of applications, such as
88 facilitating the detection of the pathogen in infection models. New tools or protocols
89 must be developed or adapted for non-model fungi such as *E. africanus.* In this study,
90 we used molecular tools originally developed for *Histoplasma capsulatum* and other
91 dimorphic fungi (6-11) and adapted them to the genetic modification of *E. africanus*.

92 In some fungi, notably the dimorphic fungal pathogens, homologous recombination is
93 inefficient, which prevents gene replacement strategies. In these cases,
94 *Agrobacterium*-mediated gene transfer (ATMT) has been employed to introduce genes
95 of interest (9, 11) or fluorescent transcriptional reporters or to create random insertion
96 libraries for phenotypic screening. Co-culture of *A. tumefaciens,* harbouring the shuttle
97 plasmid, with the fungus results in the insertion of a single copy (in the majority of
98 cases) of the T-DNA randomly in the genome (12). This method has been used
99 successfully for several of the thermally dimorphic pathogens, including *Histoplasma*
100 *capsulatum, Blastomyces dermatitidis, Paracoccidioides brasiliensis* and *Talaromyces*
101 *marneffei* (as reviewed in (13)). We used ATMT to introduce a GFP transgene into *E.*
102 *africanus,* using shuttle vectors and a protocol previously developed for the
103 transformation of *H. capsulatum* (14). The *E. africanus* GFP reporter strain facilitated
104 imaging of yeast-macrophage interactions and identification of phagocyte cell types in
105 the lung associated with the yeast in the mouse model of infection (15) by flow
106 cytometry analysis.

107 Shuttle vectors which replicate in *E. coli* can be maintained by *H. capsulatum* as linear
108 plasmids through the addition of telomere sequences (16-18). These vectors are
109 useful for introducing expression constructs without genome modification. For

110 example, RNA interference (RNAi) constructs can be used to knock down expression
111 of virulence-associated genes (7, 18-22). These plasmids are rapidly lost without
112 selection pressure, which is useful when transient expression is desired, e.g.
113 expression of the genome-modifying enzyme Cas9. Gene deletion/mutation is a
114 powerful tool to study putative virulence-associated traits. CRISPR-Cas9 genome
115 editing has been applied to study these traits in thermally pathogenic fungi, including
116 *Blastomyces dermatitidis (23)* and *Histoplasma capsulatum (6, 24).* In this study, we
117 applied an episomal plasmid system designed for *H. capsulatum* for CRISPR-Cas9
118 genome editing (6) in *E. africanus* to delete distinct genes in the genome.

119 With effective molecular genetic tools in place, and their application optimised for *E.*
120 *africanus*, its virulence traits and pathogenesis can be investigated in future work. This
121 knowledge could facilitate the development of more specific diagnostic tests for early
122 screening of at-risk patients or inform clinical management of the disease.

123

124 Results and Discussion

125 Generation of fluorescent strains using *Agrobacterium*-mediated 126 transformation of a GFP transgene

127 We used *Agrobacterium tumefaciens*-mediated transformation (ATMT) to transform *E.*
128 *africanus* using the shuttle vector pAG22, which encodes a GFP transgene. GFP and
129 hygromycin phosphotransferase are expressed under the control of *H. capsulatum*
130 regulatory elements: *TEF1* (translation elongation factor) constitutive promoter and
131 *TUB2 (tubulin)* terminator, and *RPL1B* (large ribosomal subunit protein) promoter and
132 *RPL7* (large ribosomal subunit protein) terminator, respectively. Transformation of *E.*
133 *africanus* using *A. tumefaciens* LBA1100 or EHA105 strains carrying pAG22 yielded

134 similar numbers of transformants. Following transformation, individual transformants
135 were screened for GFP expression levels, as insertion of the T-DNA in different loci
136 can result in varying levels of GFP expression (12). To identify reporter strains with
137 high GFP expression, transformant colonies were grown in liquid BHI broth and
138 inspected by fluorescence microscopy. Figure 1 shows an example of differences in
139 GFP fluorescence levels between two transformants.

140 One pAG22 transformant with high fluorescence was selected for further applications.
141 In preliminary experiments with the mouse model of infection, it was noted that the
142 virulence of laboratory-passaged *E. africanus* (including untransformed wild-type
143 strains) was reduced, as higher doses of yeast were required to replicate pathology
144 compared to previous work. Therefore, all wild-type and control strains used in this
145 study were passaged under the same conditions in the laboratory as would be required
146 to generate respective transformants. An intranasal dose of 1×10^7 yeast cells was
147 then used to infect mice, as this could replicate the pathology seen in previous work
148 (15). With these conditions, mice infected with the GFP fluorescent strain did not show
149 a difference in mortality compared to the passage-matched wild-type strain in survival
150 studies.

151

152 **Fluorescent E. africanus yeast interaction with macrophages**

153 The GFP-fluorescent yeast facilitated imaging of *E. africanus* interaction with
154 macrophages. J774A.1 macrophages in chambered imaging slides were infected with
155 *E. africanus* yeast (MOI=1) and imaged every 20 minutes. Un-opsonised yeast cells
156 are readily phagocytosed, and a high proportion of yeast cells were intracellular at the
157 start of imaging, one hour following yeast addition. We hypothesise that *E. africanus*

158 may be taken up by macrophages by the same mechanism as *H. capsulatum*, namely,
159 recognition of heat shock protein 60 (Hsp60) on the surface of yeast cells by
160 complement receptor 3 (CD11b/CD18) of macrophages (25), as Hsp60 is highly
161 conserved between the two species. Intracellular yeast could easily be observed by
162 its GFP fluorescence (Figure 2A). Budding of intracellular yeast could be measured in
163 the time-lapse data, demonstrating phagocytosed *E. africanus* yeasts remained
164 viable. The observed budding time of intracellular yeast was not significantly different
165 to that of extracellular yeast in the same proximity (Figure 2B). Yeast cells continued
166 to proliferate intracellularly over time, with some macrophages appearing heavily
167 infected and unable to control yeast proliferation. These data indicate that the
168 intracellular niche is permissive to *E. africanus* replication, as it is for *H. capsulatum.*
169 Previous work showed that bone marrow-derived macrophages are not actively lysed
170 by *E. africanus*, unlike *H. capsulatum*, which may be due to the non-lytic activity of the
171 *E. africanus* Cbp1 homologue (26). These data suggest that, similar to *H. capsulatum*
172 and *P. brasiliensis,* non-activated phagocytes are unable to control *E. africanus,* which
173 may aid in fungal systemic dissemination during infection (27, 28). Further studies
174 using the GFP reporter strain and live cell imaging could provide more information on
175 the dynamics of intracellular replication and macrophage cell death.

176

177 **Identification of infected phagocyte populations in the mouse lung following**
178 **infection with the GFP reporter strain**

179 We applied the GFP fluorescent *E. africanus* strain to examine its association with
180 phagocytes *in vivo.* Mice were infected intranasally with the fluorescent *E. africanus*
181 strain, and after 7 days, myeloid cell recruitment in the lungs was analysed by flow

182 cytometry. Lungs from uninfected mice were analysed as a control. Gating first on
183 GFP+ cells (i.e., cells with internalised E. africanus) showed that <1% of GFP+ cells
184 were CD45-negative (Figure 3A), suggesting that nearly all phagocytosed *E. africanus*
185 yeasts resided in CD45+ phagocytes. Similar results were reported in a study with an
186 *H. capsulatum* GFP-expressing strain (29), suggesting that both pathogens persist
187 well within this intracellular niche *in vivo*. However, these results only reflect the
188 intracellular fungal burden at the day 7 timepoint, and do not account for fungi that
189 may have been cleared by this time. Most GFP-fluorescent yeasts were associated
190 with neutrophils (CD11b^{hi}, Ly6G^{hi}) (66.4±17.4% of GFP+ cells; Figure 3B). The
191 remainder of cell types that contained GFP yeast were interstitial macrophages
192 (10.3±5.3%), dendritic cells (MHCII^{hi}, CD11c+) (2.1±0.7%) and a very small subset of
193 CD11b-, CD11c- cells (Figure 3B).

194 Alternatively, gating first on all live host cells showed what proportion of total cells were
195 infected with *E. africanus* (GFP+). Of CD45+ cells within the lung, approximately
196 16.4±4% were infected (GFP+). We then characterised the GFP-fluorescent (i.e.,
197 infected) proportion of each myeloid cell type, using a similar gating strategy. The
198 mean proportion of DCs that were infected (GFP-positive) was 57.3±4.3% of DCs
199 detected (MHCII^{hi}, CD11c^{hi}), with smaller proportions of total lung macrophages and
200 neutrophils infected (Figure 3C). Similar proportions were reported for *H. capsulatum*
201 with the distribution of GFP-fluorescent *H. capsulatum*-infected phagocytes at day 7
202 post-infection: macrophages: 25.1%, PMNs: 51.2% and DCs: 24.3% for the G217B
203 strain (29). DCs are pivotal in the adaptive immune response to fungi, including *H.*
204 *capsulatum* (30, 31). The high proportion of DCs infected with *E. africanus* at the 7-
205 day timepoint suggests the initiation of adaptive immunity. The cellular recruitment (of
206 CD45+ cells) to the lung in response to the GFP-fluorescent strain was not significantly

207 different to CD45+ cell populations in animals infected with the non-fluorescent wild-
208 type control (Figure 3D), indicating the GFP-fluorescent E. africanus strain stimulates
209 a similar host immune response. Previous work examined myeloid cell recruitment in
210 *E. africanus*-infected mouse lung at 14 days post-infection, although a lower dose of
211 yeast was used for infection (15). A time course of infection was not performed in the
212 current study; this could be included in future experiments to gain more information on
213 cell recruitment and infected phagocyte proportions over time.

214 SiglecF+ alveolar macrophages were detected in lungs from uninfected mice (1.5-4%
215 of total cells), but the proportion was reduced in infected mice (0.01-0.16% of total
216 cells). Similarly, the number of interstitial macrophages and dendritic cells was higher
217 in uninfected mice (Figure 3D). This could be due to the proportional increase in
218 neutrophils recruited or apoptosis of leukocytes in the lung, a known feature of
219 infection with *H. capsulatum* and a critical element of protective immunity (32).

220

221 **Transformation of *E. africanus* with episomal vectors and reduction of cell wall**
222 **α(1,3)-glucan by RNA interference**

223 *E. africanus* could be transformed with episomal plasmids based on pCR115 (18) for
224 which linear plasmids with telomeres are maintained without chromosome integration.
225 This was first tested by constructing a modified plasmid with hygromycin B selection
226 (pHygR-GFP). The number of colonies obtained using electroporation of episomal
227 plasmids was typically lower than for ATMT. Hygromycin selection pressure was
228 maintained when working with these transformants, as these plasmids are rapidly lost
229 from the cell population without selection.

230 To silence production of α(1,3)-glucan in *E. africanus*, we expressed an AGS1-
231 targeting RNA hairpin from an episomal plasmid based on the AGS1-RNAi plasmid
232 pCR115. The RNA hairpin is designed for RNAi-induced knockdown of the *H.*
233 *capsulatum AGS1* gene, with homology to a 678-base pair region of exon 3 of this
234 gene (18). This region is 84% similar overall in *H. capsulatum* and *E. africanus,* with
235 several continuous sections of at least 20 nucleotides or with 100% identity. Therefore,
236 we hypothesised that effective RNAi silencing using the same RNA hairpin could be
237 achieved in *E. africanus,* given that several 21-22 small interfering RNA molecules
238 with complete sequence match are produced following Dicer processing of the long
239 double-stranded RNA. We replaced the GFP in pHygR-GFP with the *AGS1* inverted
240 repeat sequence from pCR115 and used this plasmid (pHygR-HcAGS1-RNAi) to
241 transform *E. africanus.* Yeast transformed with pHygR-HcAGS1-RNAi did not differ in
242 growth rate compared to control yeast, which was transformed with a similar plasmid
243 containing a GFP inverted repeat.

244 Reduction of cell wall α(1,3)-glucan through RNA interference was assessed by
245 staining the AGS1-RNAi plasmid-transformed yeasts with a monoclonal antibody
246 recognising α(1,3)-glucan. It was noted that not all yeast cells were uniformly stained
247 (Figure 4A), suggesting variable amounts of α(1,3)-glucan. *H. capsulatum* also
248 displays variation in cell wall α(1,3)-glucan levels, as assessed by staining with the
249 same antibody, during broth culture growth (33). Similarly, *E. africanus* cell wall α(1,3)-
250 glucan levels may increase at different time points during culture, or in different growth
251 media. Nevertheless, yeasts transformed with the *AGS1* RNAi plasmid showed an
252 overall lower level of cell wall α(1,3)-glucan staining in the population compared to the
253 control (Figure 4A and 4B). RNAi-induced gene silencing does not typically lead to a
254 complete knockdown of the target, and due to variability in dsRNA expression, a small

255 proportion of cells do not exhibit the full RNAi effect (18). Therefore, some α(1,3)-
256 glucan staining was still observed in *E. africanus* yeasts maintaining the RNAi plasmid.

257

258 **Gene mutation in *E. africanus* using an episomal CRISPR/Cas9 system**

259 To test whether CRISPR-Cas9 gene editing could facilitate gene mutation in E.
260 africanus, we transformed a GFP-expressing strain of *E. africanus* with a linear
261 plasmid expressing Cas9 and a GFP-targeting CRISPR gRNA. The GFP-fluorescent
262 *E. africanus* strain was generated through ATMT using pAG21 (GFP-expression and
263 G418 selection). The CRISPR-Cas9 plasmid provided for hygromycin resistance and
264 expressed a gRNA targeting the GFP gene. Hygromycin-resistant transformant
265 colonies were passaged in BHI broth with hygromycin B selection, and the yeasts were
266 examined by fluorescence microscopy for loss of the GFP fluorescence. After
267 successive passages, an increasing proportion of the population was no longer GFP
268 fluorescent (Figure 5A). Sequencing of the GFP gene in the transformant population
269 confirmed a mixed population with indels at the expected Cas9 cut site (Figure 5B),
270 showing efficient CRISPR/Cas9-based genome editing in *E. africanus*.

271 Auxotroph strains are useful for genetic manipulations because they facilitate the
272 selection of plasmids carrying genes that rescue the auxotrophy. A previous
273 CRISPR/Cas9 workflow used for *H. capsulatum* (6) was used to disrupt *URA5* in *E.*
274 *africanus* to generate a uracil auxotroph strain. The *E. africanus URA5* homologue
275 (Gene: ACJ72_02173) was identified through a BLAST search. The protein sequence
276 is highly similar to that of *H. capsulatum* (88.1% identity, 93.0% similarity as
277 determined by pairwise alignment using EMBOSS Water (34)). A guide RNA sequence
278 was designed using CRISPOR (https://crispor.gi.ucsc.edu/) (35) to maximise the

279 chance of indel generation in the *URA5* gene while minimising off-target effects.
280 Following transformation of wild-type *E. africanus* with the URA5-targeting CRISPR-
281 Cas9 plasmid, followed by four passages under hygromycin selection, uracil
282 auxotrophs were selected using 5-FOA-resistance screening. Several 5-FOA-resistant
283 clones were identified, and their inability to grow without uracil was validated by failure
284 to grow in media lacking uracil. Sequencing of four clones showed a single nucleotide
285 T insertion in all clones (Figure 5C), causing a frameshift mutation, preventing
286 production of a functional *URA5* gene product. This *E. africanus ura5*-mutant can now
287 be used as the host for *URA5*-based expression vectors or RNAi vectors. These
288 vectors are also stable *in vivo,* as evidenced by continued virulence*; H. capsulatum*
289 uracil auxotrophs are avirulent in mice, which is likely to be the case for *E. africanus*
290 as well (36).

291

292 ## Conclusions

293 In this study, we demonstrate that molecular tools developed for genetic modification
294 of *H. capsulatum* could be adapted for use in *E. africanus,* suggesting that the two
295 species use similar regulatory elements for high-level gene expression. Our results
296 include the use of ATMT to transform *E. africanus* with expression plasmids,
297 generating a GFP-fluorescent strain that can be used for tracking infections both in
298 cultured macrophages and *in vivo*. In addition, we provide results showing the efficacy
299 of episomal plasmids designed to induce RNA-interference-based gene knockdown
300 and CRISPR-Cas9-based mutation of target genes. Thus, by adapting technologies,
301 we have put into place tools and methodologies to functionally study genes in E.
302 africanus through expression as well as loss-of-function. Furthermore, we have

303 created an *E. africanus* uracil auxotroph strain enabling the use of URA5-based
304 complementation vectors instead of hygromycin selection. Such URA5-based vectors
305 have the advantage of providing for selection *in vivo*, which cannot be done with
306 hygromycin. Together, these tools make *E. africanus* amenable to genetic modification
307 to investigate virulence traits and how they influence the host-pathogen interaction.

308

309 Materials and Methods

310 *E. africanus* and *A. tumefaciens* strains and growth conditions

311 *Emergomyces africanus* (clinical isolate CBS 136260 (4)) was grown in brain-heart
312 infusion broth (BHI) (Cat No. 110493, Merck, USA), at 37 °C, 180 rpm, or maintained
313 on BHI agar plates (Cat. No. 70138, Merck) at 37 °C. *A. tumefaciens* strains LBA1100
314 and EHA105 were maintained on LB agar plates at 25 °C. Transformation of
315 *Agrobacterium* binary vectors into *A. tumefaciens* was done by electroporation as
316 described in (37) and transformants selected with 100 µg/mL kanamycin.

317

318 Transformation using *Agrobacterium tumefaciens*

319 Transformation of *E. africanus* yeast by *Agrobacterium* was done using previously
320 established methods for *H. capsulatum* (14), with the exception that BHI broth or BHI
321 agar plates were used instead of *Histoplasma*-specific growth medium. *Agrobacterium*
322 *tumefaciens* strains LBA1100 and EHA105 were used to transform *E. africanus* with
323 pAG22 (GFP-expression, hygromycin resistance), yielding similar results. BHI was
324 inoculated with a colony of *E. africanus* from a fresh streak plate, and the culture was
325 grown for three days at 37 °C with shaking. Colonies from a streak plate of *A.*

326 *tumefaciens* were used to inoculate 5 ml minimal glucose medium (14) for 24 h at 25
327 °C, then 1 ml of this culture was used to inoculate 5 ml induction medium containing
328 0.1 mM acetosyringone (Sigma-Aldrich) for a further 16 h of growth. *E. africanus* yeast
329 cells were washed with PBS by centrifugation and resuspension, then resuspended in
330 induction medium. The optical density (600 nm) of both *E. africanus* and *A.*
331 *tumefaciens* suspensions was determined, then combined in 900 µl to give final optical
332 densities of 1.0 for each. Suspensions OD600=1.0 have approximately 5×10^8 cells/ml
333 and 2.5×10^8 cells/ml of *A. tumefaciens* and *E. africanus,* respectively, giving an MOI
334 of 2:1. The co-culture was applied dropwise to sterile Whatman No. 5 qualitative filter
335 papers placed on co-cultivation plates. The co-cultivation plates were incubated at 25
336 °C for 2 days, then transferred to BHI agar plates containing 300 µg/ml hygromycin B
337 and 200 µM cefotaxime. The plates were incubated at 37 °C for 10-14 days until *E.*
338 *africanus* transformant colonies appeared. Single colonies were picked and streaked
339 on fresh BHI plates containing 300 µg/ml hygromycin B. From these plates, single
340 colonies were used to inoculate BHI broth to grow liquid cultures of individual
341 transformants. Glycerol stocks (20%) of liquid cultures were preserved at -80 °C.

342

343 **Infection of macrophages with *E. africanus* and live-cell imaging**

344 J774A.1 murine macrophage cells (ATCC: TIB-7) were seeded at a density of 2×10^5
345 cells in 0.3 ml macrophage medium (DMEM high glucose GlutaMAX®, 10% FBS,
346 penicillin/streptomycin [Gibco]) in 8-well imaging slides (ibidi GMBH, Cat. No. 80826)
347 24 h prior to the addition of *E. africanus* yeast. *E. africanus* yeast was grown for 3 days
348 in BHI broth, then washed with PBS and counted using a haemocytometer. 2×10^5
349 yeast cells in 300 µl macrophage media were added to macrophages in imaging slides

350 to achieve a ratio of one yeast cell per macrophage (MOI=1). The slides were then set
351 up for time-lapse imaging under the conditions of 37 °C, 5% CO_2. Imaging was started
352 1 hour post-yeast addition. Imaging was done using a Zeiss AxioObserver
353 fluorescence microscope at 40X magnification. Analysis of observed budding time was
354 done by examining yeast cells that were intracellular or extracellular, at t=0, with no
355 visible buds.

356

357 **Mouse model of infection and flow cytometry**

358 To examine the responses to *E. africanus* in the mouse lung, three groups of mice
359 were analysed (n=6 per group): (1) uninfected mice, (2) mice infected with the wild-
360 type clinical isolate and (3) mice infected with the GFP fluorescent *E. africanus* strain.
361 Eight- to twelve-week-old male CL57/B6 mice were obtained from the University of
362 Cape Town Animal Research Specific Pathogen Free Facility. *E. africanus* wild-type
363 and GFP fluorescent strains were grown in BHI broth for 3 days at 37 °C until OD600
364 reached approximately 1.0. Yeast cells were washed twice with PBS before counting
365 using a haemocytometer. Mice were anaesthetised with ketamine and xylazine (80
366 mg/kg and 16 mg/kg, respectively), then infected intranasally with 50 µl of yeast cell
367 suspension containing 1×10^7 yeast cells. Animal welfare was monitored daily. After 7
368 days, mice were euthanised by halothane inhalation and the lungs were removed and
369 stored in DMEM + 5% FBS on ice. Lungs were digested in digestion buffer (15)
370 containing 50 units/ml Collagenase Type I and 13 µg/ml DNAse I for 1h at 37 °C. The
371 digested lungs were passed through a 70 µm cell strainer using a sterile syringe
372 plunger. This process was repeated using a 40 µm cell strainer. Red blood cells were
373 lysed using 1x RBC lysis buffer (eBioscience), then remaining cells collected by

374 centrifugation and resuspension in DMEM + 5% FBS, then counted using a
375 haemocytometer. 2 × 10^6 cells per well were added to a V-bottom 96-well plate.
376 Myeloid cells were stained in MACS buffer (0.5% BSA, 2 mM EDTA in PBS) using the
377 antibodies in Table 3, together with 1% Fc block and 2% heat-inactivated rat serum,
378 for 20 min at 4 °C in the dark, then washed twice with MACS buffer. 7-AAD (Biolegend)
379 was used as the cell viability stain. Single-stained and unstained controls were used
380 to compensate for spectral overlap. Stained cells were analysed by flow cytometry
381 using an LSR Fortessa™ (BD Immunocytometry Systems, San Jose, CA, USA) and
382 BD FACS Diva software (v6.0). Flowjo software (v10.0.7) (Treestar, Ashland, OR,
383 USA) was used for post-acquisition analysis and cell population determination. The
384 gating strategy used is shown in Figure 3A.

385

386

387 **Plasmid construction**

388 Plasmids pAG21, pAG22, pCR115 (18), pSL01 and pCR745 (6) were provided by
389 CAR. Isolation of plasmid DNA, restriction enzyme cloning and PCR/gel purification
390 were done using standard methods, and plasmids were maintained in *E. coli* DH5α.
391 Restriction enzymes and ligation kits were purchased from New England Biolabs. An
392 episomal GFP expression plasmid (pHygR-GFP) was constructed by digestion of
393 pAG22 with EcoRI and HindIII, and ligating the fragment containing the GFP- and *hph*
394 expression cassettes into the similarly-digested pCR115 vector backbone. To
395 construct pHyg-HcAGS1-RNAi (AGS1 inverted repeat) used for *AGS1* RNAi, the *GFP*
396 sequence from plasmid pHygR-GFP was exchanged with the *AGS1* inverted repeat
397 sequence from pCR115 by digestion with AscI and SpeI. A control *GFP* RNAi plasmid

398 (pHygR-GFP-RNAi) was constructed by inserting an inverted repeat of *GFP* into
399 pHygR-GFP by PCR with GFP-SpeI-F and XhoI-GFP-R primers and restriction
400 enzyme cloning. For CRISPR/Cas9-mediated disruption of GFP, plasmid pCR115-
401 sgGFP was created: a portion of plasmid pCR745 (6) containing the guide RNA
402 targeting GFP was digested with SwaI and AvrII and ligated into similarly digested
403 pSL01 (6), resulting in plasmid pSL01-sgGFP. For CRISPR/Cas9-mediated disruption
404 of *URA5,* a synthetic DNA sequence containing the guide RNA sequence,
405 hammerhead and HDV ribozyme sequences, and part of the tracr RNA sequence,
406 including 15 bp up- and downstream-homology regions, was designed for cloning into
407 pSL01 as described in (6). The guide RNA sequence was designed using CRISPOR
408 (https://crispor.gi.ucsc.edu/) (35) to maximise the chance of indels while preventing
409 off-target effects. This sequence was synthesised by Integrated DNA Technologies
410 (Leuven, Belgium). The synthetic DNA sequence was cloned into SwaI-digested
411 pSL01 and transformed into competent *E. coli* cells using In-Fusion® HD Cloning Kit
412 (Takara Bio) using the manufacturer's recommendations.

413

414 **Transformation of yeast with episomal plasmids by electroporation**

415 Transformation of *E. africanus* with plasmids by electroporation of was based on
416 previously established methods for *H. capsulatum* (17). Briefly, *E. africanus* yeasts
417 were grown in 5 ml BHI broth for 3 days until OD600 reached approximately 1.0. Yeast
418 cells were collected by centrifugation and resuspended in 2 ml 10% mannitol.
419 Plasmids were linearised by digestion with PmeI to expose the telomeres, then
420 column-purified and eluted with nuclease-free water. Three hundred microlitres of *E.*
421 *africanus* yeast suspension (1×10^7 yeast cells) was mixed with 200 ng purified

422 plasmid in a chilled electroporation cuvette (0.2 cm gap), then electroporated in a
423 single pulse using a Bio-Rad Gene Pulser® II system with the following settings: 1.25
424 kV, 50 mF, 600 Ω, which gave a time constant of 8-12 ms. Following electroporation,
425 500 µl of BHI broth was mixed with cells and this cell suspension was applied dropwise
426 to sterile Whatman No. 5 qualitative filter papers placed on BHI agar plates with no
427 selection. These plates were incubated for 48 h at 37 °C to allow for recovery of
428 transformants, before transferring the membranes to BHI agar plates containing 300
429 µg/ml hygromycin B. The plates were incubated at 37 °C for 10-14 days until
430 transformant colonies appeared. Single colonies were picked and streaked onto fresh
431 BHI plates (300 µg/ml hygromycin B). Selection with hygromycin B (300 µg/ml) was
432 maintained for growing liquid cultures, after which -80 °C glycerol stocks were
433 prepared for long-term storage of strains, as described above.

434

435 **Cell wall alpha(1,3)-glucan staining of RNAi strains**

436 Yeasts harbouring the *AGS1* RNAi plasmid pHygR-HcAGS1-RNAi or the control
437 plasmid pHygR-GFP-RNAi were grown for 3 days in BHI broth with 300 µg/ml
438 hygromycin B until cell density reached an OD600 of 1.0. Cells from 300 µl of culture
439 were collected by centrifugation, then washed twice with PBS, and fixed in 4%
440 paraformaldehyde overnight at 4 °C. Cells were washed twice with PBS, then blocked
441 with 1% BSA, PBS for 1 h. Cells were then stained with 1:150 mouse IgM MOPC-
442 104E antibody (M5170, Sigma-Aldrich) in 1% BSA, PBS for 2 h at ambient
443 temperature. The cells were washed twice by centrifugation and resuspended in PBS
444 and stained with 1:400 anti-mouse IgM secondary antibody conjugated to
445 AlexaFluor488 (Invitrogen, A-21042) for 1 h at ambient temperature. To stain total

446 yeast cells, calcofluor white was added at a final concentration of 100 µg/ml and
447 incubated for 15 min at ambient temperature in the dark. Cells were washed twice with
448 PBS and resuspended in 20 µl PBS. A 5µl sample of stained cells was spotted onto a
449 microscope slide, allowed to air-dry and mounted with ProLong™ Glass Antifade
450 Mountant (P36984, Invitrogen). The slides were examined using a Zeiss Axiovert
451 200M fluorescence microscope with a monochrome Zeiss AxioCam HRm camera at
452 100x magnification. Exposure times were kept constant for all samples when capturing
453 images for mean fluorescence analysis. Fluorescence of the population was
454 determined by measuring the background-corrected mean grey values for 10 fields of
455 view each using ImageJ, for two pooled independent experiments, then dividing this
456 value by the number of total cells (as determined by calcofluor white staining).

457

458

459 **Targeted mutagenesis using CRISPR/Cas9-plasmids**

460 A GFP-expressing strain of *E. africanus* was generated through ATMT using pAG21
461 (equivalent to pAG22 but with a G418 resistance marker instead of hygromycin B
462 resistance). The GFP-fluorescent strain was subsequently transformed with PmeI-
463 linearised plasmid pSL01-sgGFP by electroporation. Hygromycin-resistant
464 transformant colonies were picked and grown in BHI broth for successive passages
465 (1:50 dilution), maintaining hygromycin selection every 3 days. Samples of these
466 cultures were examined by fluorescence microscopy for GFP expression. For DNA
467 sequencing, yeast cells from 1 ml of culture was collected by centrifugation, lysed with
468 200 µl of lysis buffer (2% Triton X-100, 20 mM EDTA) and beating (2 min) with
469 approximately 100 µl of glass beads (0.5 µm diameter). 100 µL of phenol and 100 µl

470 chloroform-isoamyl alcohol (25:24:1) were added, and the phases were separated by
471 centrifugation. DNA was recovered by transferring 50 µl of the aqueous (upper) phase
472 into 200 µl distilled water. This crude DNA-containing solution was used as the
473 template (2% vol/vol) for PCR using Taq polymerase and primers flanking the
474 expected gene editing sites: GFP-SpeI-F and GFP-Xho-R, or Ura seq-F and Ura seq-
475 R.

476 For mutation of *URA5* to create a uracil auxotroph, a guide RNA sequence targeting
477 URA5 was designed using CRISPOR (https://crispor.gi.ucsc.edu/) (35). A DNA
478 construct containing the crRNA, hammerhead- and HDV ribozyme sequences, and
479 part of the tracrRNA sequence, with 15 bp flanking homology arms, was synthesised
480 as described in (6) for cloning into plasmid pSL01, by Integrated DNA Technologies
481 (Leuven, Belgium). The sequence of this construct is shown in Table 2. Cloning of this
482 synthetic DNA into SwaI-digested plasmid pSL01 was done through InFusion Cloning
483 (Takara Biotec) as per the manufacturer's recommendations. Constructs were verified
484 through Sanger sequencing. *E. africanus* was transformed with this plasmid by
485 electroporation as described above, followed by selection with hygromycin B. After
486 four passages in liquid culture, cultures were streaked onto BHI plates supplemented
487 with 1mg/ml 5-Fluoroorotic Acid (5-FOA, R0811, ThermoFisher) and 100 µg/ml uracil
488 to isolate uracil auxotrophs. Uracil auxotrophy was confirmed by the inability to grow
489 in DMEM/F12 media (11320033, Gibco), which lacks uracil, compared to growth in
490 parallel in DMEM/F12 media supplemented with 100 µg/ml uracil. Independent clones
491 were picked for Sanger sequencing.

492

493

494 **Ethics statement**

495 All work with mice was done with ethical clearance from the University of Cape Town
496 Animal Research Ethics Committee, reference number 020/017.

497

498 **Statistical analysis and software**

499 Values are reported as means ± standard deviation. Differences between groups were
500 determined using a two-tailed Student's t-test or one-way ANOVA using GraphPad
501 Prism v10.6.1. Plasmid map generation and alignments of DNA sequence data were
502 done using SnapGene v8.02. ImageJ 1.54p was used for image analysis (mean
503 fluorescence intensities and total cell counting).

504

505 **Funding statement**

506 This work was supported by the National Research Foundation of South Africa (to
507 JCH), Carnegie Corporation (to JCH and LD), National Institute of Allergy and
508 Infectious Diseases (NIAID) AI148561 to CAR, and Wellcome Trust: 209293/Z/17/Z to
509 JCH and 310933/Z/24/Z to ERB and JCH. The funders played no role in the study
510 design, data collection and analysis, decision to publish, or preparation of the
511 manuscript.

512

513 **Competing Interest Statement**

514 The authors have declared no competing interest.

515

516

517 Table 1: Plasmids used in the study

518

Plasmid	Application	Selection
pAG22	ATMT	Hygromycin B (300 µg/ml)
pAG21	ATMT	G418 (1 mg/ml)
pCR115	*AGS1* RNAi	[Uracil auxotrophy]
pHygR-GFP	GFP episomal plasmid	Hygromycin B (300 µg/ml)
pHygR-GFP-RNAi	GFP inverted repeat plasmid (RNAi control)	Hygromycin B (300 µg/ml)
pHygR-HcAGS1-RNAi	*AGS1* RNAi	Hygromycin B (300 µg/ml)
pCR745	CRISPR/Cas9	[Uracil auxotrophy]
pSL01	CRISPR/Cas9	Hygromycin B (300 µg/ml)
pSL01-sgGFP	CRISPR/Cas9	Hygromycin B (300 µg/ml)
pSL01-sgURA	CRISPR/Cas9	Hygromycin B (300 µg/ml)

519

520

521

522 Table 2: Primers and oligonucleotides

GFP-SpeIF	GAGAACTAGTATGAGCAAGGGCGAGGAGC
GFP-XhoIR	GAGACTCGAGCTTGTACAGCTCGTCCATGC
Synthesised sequence for *URA5* CRISPR/Cas9 editing (guide sequence underlined)	CTCTCCCAATTTTCACATTTAAATCCCGCC ACCCGATGTCTGATGAGTCCGTGAGGAC GAAACGAGTAAGCTCGTC<u>ACATCGGGTT TCGGAATGG</u>AGTTTTAGAGCTAGAAATAG CAAGTTAAAATAAGGCTAGTCCGTTAT
Ura seq F	TTGACACAGCCCATAAACG
Ura seq R	ATCGCCTTCTATATTCCTCC

523

524

525

526

527

528

529

530

531 Table 3: Flow cytometry antibodies

Target (Clone)	Conjugated fluorophore	Manufacturer (catalogue number)	Dilution
CD45 (30-F11)	BV510	BD Biosciences (567800)	1:100
CD11b (M1/70)	BV421	BD Biosciences (566313)	1:100
CD11c (HL3)	Alexa Fluor 700	BD Biosciences (560583)	1:100
Ly-6G (1A8)	APC	BD Biosciences (560599)	1:100
F4/80 (BM8)	PE/Cy7	Biolegend (123113)	1:100
Siglec-F (E50-2440)	APC/Cy7	BD Biosciences (565527)	1:50
I-A/I-E (MHCII) (M5/114.15.2)	PE/Cy5	Biolegend (107611)	1:100

532

533

534

535

536

537

538

539

540

541

542

543

544

545

546

547

548

549

References

1. Dukik K, Munoz JF, Jiang Y, Feng P, Sigler L, Stielow JB, Freeke J, Jamalian A, Gerrits van den Ende B, McEwen JG, Clay OK, Schwartz IS, Govender NP, Maphanga TG, Cuomo CA, Moreno LF, Kenyon C, Borman AM, de Hoog S. 2017. Novel taxa of thermally dimorphic systemic pathogens in the Ajellomycetaceae (Onygenales). Mycoses 60:296-309.
2. Schwartz IS, Govender NP, Sigler L, Jiang Y, Maphanga TG, Toplis B, Botha A, Dukik K, Hoving JC, Munoz JF, de Hoog S, Cuomo CA, Colebunders R, Kenyon C. 2019. Emergomyces: The global rise of new dimorphic fungal pathogens. PLoS Pathog 15:e1007977.
3. Schwartz IS, Kenyon C, Lehloenya R, Claasens S, Spengane Z, Prozesky H, Burton R, Parker A, Wasserman S, Meintjes G, Mendelson M, Taljaard J, Schneider JW, Beylis N, Maloba B, Govender NP, Colebunders R, Dlamini S. 2017. AIDS-Related Endemic Mycoses in Western Cape, South Africa, and Clinical Mimics: A Cross-Sectional Study of Adults With Advanced HIV and Recent-Onset, Widespread Skin Lesions. Open Forum Infect Dis 4:ofx186.
4. Schwartz IS, McLoud JD, Berman D, Botha A, Lerm B, Colebunders R, Levetin E, Kenyon C. 2018. Molecular detection of airborne Emergomyces africanus, a thermally dimorphic fungal pathogen, in Cape Town, South Africa. PLoS Negl Trop Dis 12:e0006174.
5. Jiang Y, Dukik K, Muñoz JF, Sigler L, Schwartz IS, Govender NP, Kenyon C, Feng P, van den Ende BG, Stielow JB, Stchigel AM, Lu H, de Hoog S. 2018. Phylogeny, ecology and taxonomy of systemic pathogens and their relatives in Ajellomycetaceae (Onygenales): Blastomyces, Emergomyces, Emmonsia, Emmonsiellopsis. Fungal Diversity 90:245-291.
6. Rappleye CA. 2023. Targeted gene deletions in the dimorphic fungal pathogen Histoplasma using an optimized episomal CRISPR/Cas9 system. mSphere 8:e0017823.
7. Brechting PJ, Shah C, Rakotondraibe L, Shen Q, Rappleye CA. 2023. Histoplasma capsulatum requires peroxisomes for multiple virulence functions including siderophore biosynthesis. mBio 14:e0328422.
8. Kujoth GC, Sullivan TD, Klein BS. 2020. Gene Editing in Dimorphic Fungi Using CRISPR/Cas9. Curr Protoc Microbiol 59:e132.
9. Kemski MM, Stevens B, Rappleye CA. 2013. Spectrum of T-DNA integrations for insertional mutagenesis of Histoplasma capsulatum. Fungal Biol 117:41-51.
10. Youseff BH, Rappleye CA. 2012. RNAi-based gene silencing using a GFP sentinel system in Histoplasma capsulatum. Methods Mol Biol 845:151-64.
11. Sullivan TD, Rooney PJ, Klein BS. 2002. Agrobacterium tumefaciens integrates transfer DNA into single chromosomal sites of dimorphic fungi and yields homokaryotic progeny from multinucleate yeast. Eukaryot Cell 1:895-905.
12. Idnurm A, Bailey AM, Cairns TC, Elliott CE, Foster GD, Ianiri G, Jeon J. 2017. A silver bullet in a golden age of functional genomics: the impact of Agrobacterium-mediated transformation of fungi. Fungal Biol Biotechnol 4:6.

596 13. Sil A, Andrianopoulos A. 2014. Thermally Dimorphic Human Fungal
597 Pathogens--Polyphyletic Pathogens with a Convergent Pathogenicity Trait.
598 Cold Spring Harb Perspect Med 5:a019794.
599 14. Zemska O, Rappleye CA. 2012. Agrobacterium-Mediated Insertional
600 Mutagenesis in Histoplasma capsulatum, p 51-66, Host-Fungus Interactions
601 doi:10.1007/978-1-61779-539-8_4. Humana Press.
602 15. Hoft MA, Duvenage L, Salie S, Keeton R, Botha A, Schwartz IS, Govender
603 NP, Brown GD, Hoving JC. 2024. The pathogenesis of experimental
604 Emergomycosis in mice. PLoS Negl Trop Dis 18:e0011850.
605 16. Woods JP, Goldman WE. 1993. Autonomous replication of foreign DNA in
606 Histoplasma capsulatum: role of native telomeric sequences. J Bacteriol
607 175:636-41.
608 17. Woods JP, Heinecke EL, Goldman WE. 1998. Electrotransformation and
609 expression of bacterial genes encoding hygromycin phosphotransferase and
610 beta-galactosidase in the pathogenic fungus Histoplasma capsulatum. Infect
611 Immun 66:1697-707.
612 18. Rappleye CA, Engle JT, Goldman WE. 2004. RNA interference in Histoplasma
613 capsulatum demonstrates a role for alpha-(1,3)-glucan in virulence. Mol
614 Microbiol 53:153-65.
615 19. Ray SC, Rappleye CA. 2022. Mac1-Dependent Copper Sensing Promotes
616 Histoplasma Adaptation to the Phagosome during Adaptive Immunity. mBio
617 13:e0377321.
618 20. Shen Q, Ray SC, Evans HM, Deepe GS, Jr., Rappleye CA. 2020. Metabolism
619 of Gluconeogenic Substrates by an Intracellular Fungal Pathogen
620 Circumvents Nutritional Limitations within Macrophages. mBio 11.
621 21. Dade J, DuBois JC, Pasula R, Donnell AM, Caruso JA, Smulian AG, Deepe
622 GS, Jr. 2016. HcZrt2, a zinc responsive gene, is indispensable for the survival
623 of Histoplasma capsulatum in vivo. Med Mycol 54:865-75.
624 22. Hilty J, George Smulian A, Newman SL. 2011. Histoplasma capsulatum
625 utilizes siderophores for intracellular iron acquisition in macrophages. Med
626 Mycol 49:633-42.
627 23. Kujoth GC, Sullivan TD, Merkhofer R, Lee TJ, Wang H, Brandhorst T,
628 Wuthrich M, Klein BS. 2018. CRISPR/Cas9-Mediated Gene Disruption
629 Reveals the Importance of Zinc Metabolism for Fitness of the Dimorphic
630 Fungal Pathogen Blastomyces dermatitidis. mBio 9.
631 24. Joehnk B, Ali N, Voorhies M, Walcott K, Sil A. 2023. Recyclable
632 CRISPR/Cas9-mediated gene disruption and deletions in Histoplasma.
633 mSphere 8:e0037023.
634 25. Long KH, Gomez FJ, Morris RE, Newman SL. 2003. Identification of heat
635 shock protein 60 as the ligand on Histoplasma capsulatum that mediates
636 binding to CD18 receptors on human macrophages. J Immunol 170:487-94.
637 26. Azimova D, Herrera N, Duvenage L, Voorhies M, Rodriguez RA, English BC,
638 Hoving JC, Rosenberg O, Sil A. 2022. Cbp1, a fungal virulence factor under
639 positive selection, forms an effector complex that drives macrophage lysis.
640 PLoS Pathog 18:e1010417.
641 27. Allendoerfer R, Deepe GS, Jr. 1997. Intrapulmonary response to Histoplasma
642 capsulatum in gamma interferon knockout mice. Infect Immun 65:2564-9.
643 28. Calich VL, da Costa TA, Felonato M, Arruda C, Bernardino S, Loures FV,
644 Ribeiro LR, de Cássia Valente-Ferreira R, Pina A. 2008. Innate immunity to
645 Paracoccidioides brasiliensis infection. Mycopathologia 165:223-36.

646 29. Deepe GS, Jr., Gibbons RS, Smulian AG. 2008. Histoplasma capsulatum
647 manifests preferential invasion of phagocytic subpopulations in murine lungs.
648 J Leukoc Biol 84:669-78.
649 30. Van Prooyen N, Henderson CA, Hocking Murray D, Sil A. 2016. CD103+
650 Conventional Dendritic Cells Are Critical for TLR7/9-Dependent Host Defense
651 against Histoplasma capsulatum, an Endemic Fungal Pathogen of Humans.
652 PLOS Pathogens 12:e1005749.
653 31. Szymczak WA, Deepe GS, Jr. 2010. Antigen-presenting dendritic cells rescue
654 CD4-depleted CCR2-/- mice from lethal Histoplasma capsulatum infection.
655 Infect Immun 78:2125-37.
656 32. Allen HL, Deepe GS, Jr. 2005. Apoptosis modulates protective immunity to the
657 pathogenic fungus Histoplasma capsulatum. J Clin Invest 115:2875-85.
658 33. Kugler S, Schurtz Sebghati T, Groppe Eissenberg L, Goldman WE. 2000.
659 Phenotypic variation and intracellular parasitism by Histoplasma capsulatum.
660 Proc Natl Acad Sci U S A 97:8794-8.
661 34. Rice P, Longden I, Bleasby A. 2000. EMBOSS: the European Molecular
662 Biology Open Software Suite. Trends Genet 16:276-7.
663 35. Concordet JP, Haeussler M. 2018. CRISPOR: intuitive guide selection for
664 CRISPR/Cas9 genome editing experiments and screens. Nucleic Acids Res
665 46:W242-W245.
666 36. Retallack DM, Heinecke EL, Gibbons R, Deepe GS, Jr., Woods JP. 1999. The
667 URA5 gene is necessary for histoplasma capsulatum growth during infection
668 of mouse and human cells. Infect Immun 67:624-9.
669 37. den Dulk-Ras A, Hooykaas PJ. 1995. Electroporation of Agrobacterium
670 tumefaciens. Methods Mol Biol 55:63-72.

671

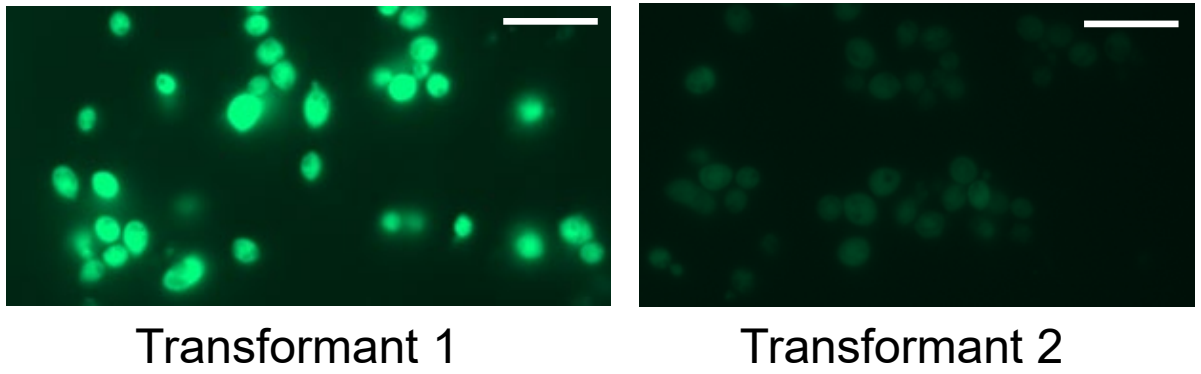

Figure 1: GFP-expressing E. africanus derived through ATMT. E. africanus GFP-expressing transformants were derived by transformation with A. tumefaciens harbouring pAG22. Individual transformant colonies were evaluated by fluorescence microscopy, showing variable expression levels of GFP between transformants under constant imaging conditions. Bar=10μm

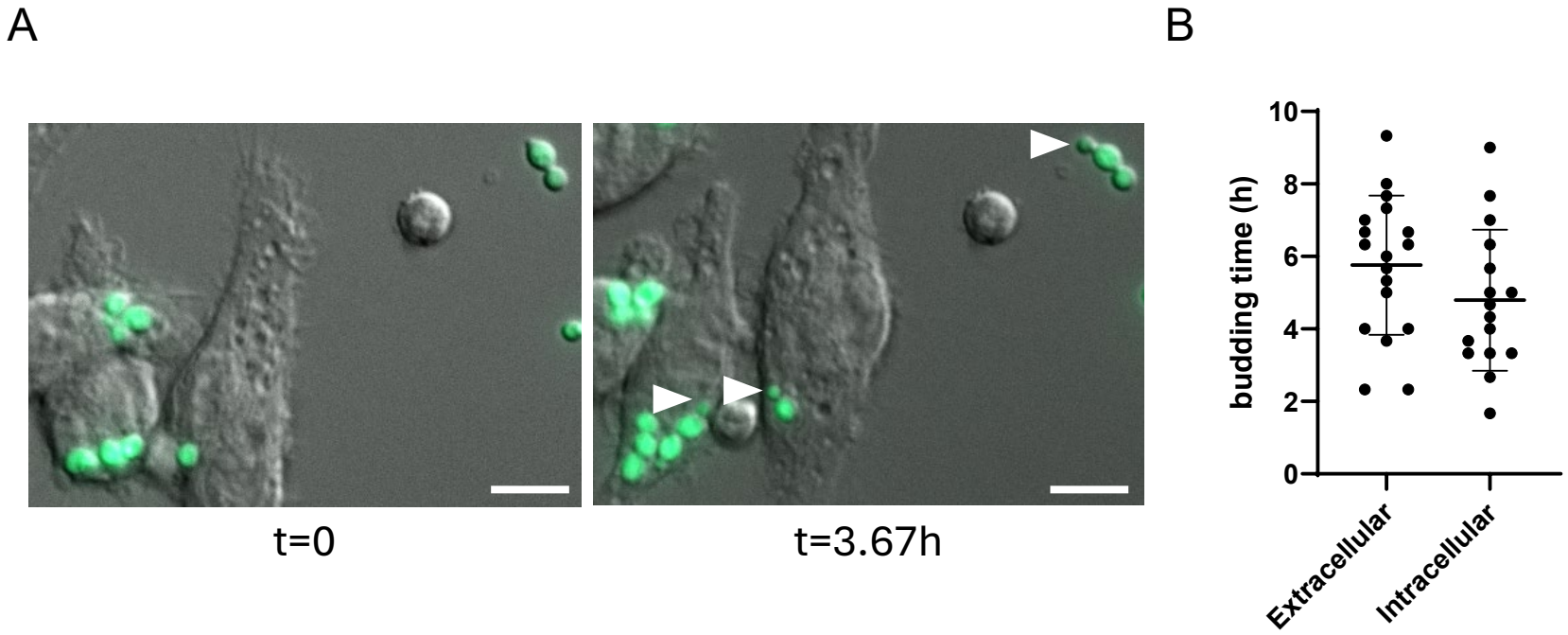

Figure 2: An *E. africanus* GFP fluorescent reporter strain facilitates the study of intracellular yeast growth
GFP fluorescent reporter yeast was added to J774.1 macrophage cells in chambered imaging slides. Time-lapse imaging was started 1 hour after yeast addition (t=0), at which point several yeast cells had been internalised (a representative example is shown in A, left). The emergence of new buds (A, right, indicated by arrows) was recorded. Observed budding time was summarised for several fields of view that contained a mix of both extracellular and intracellular yeasts, $P>0.05$ (mean ± SD). Bar=10μm.

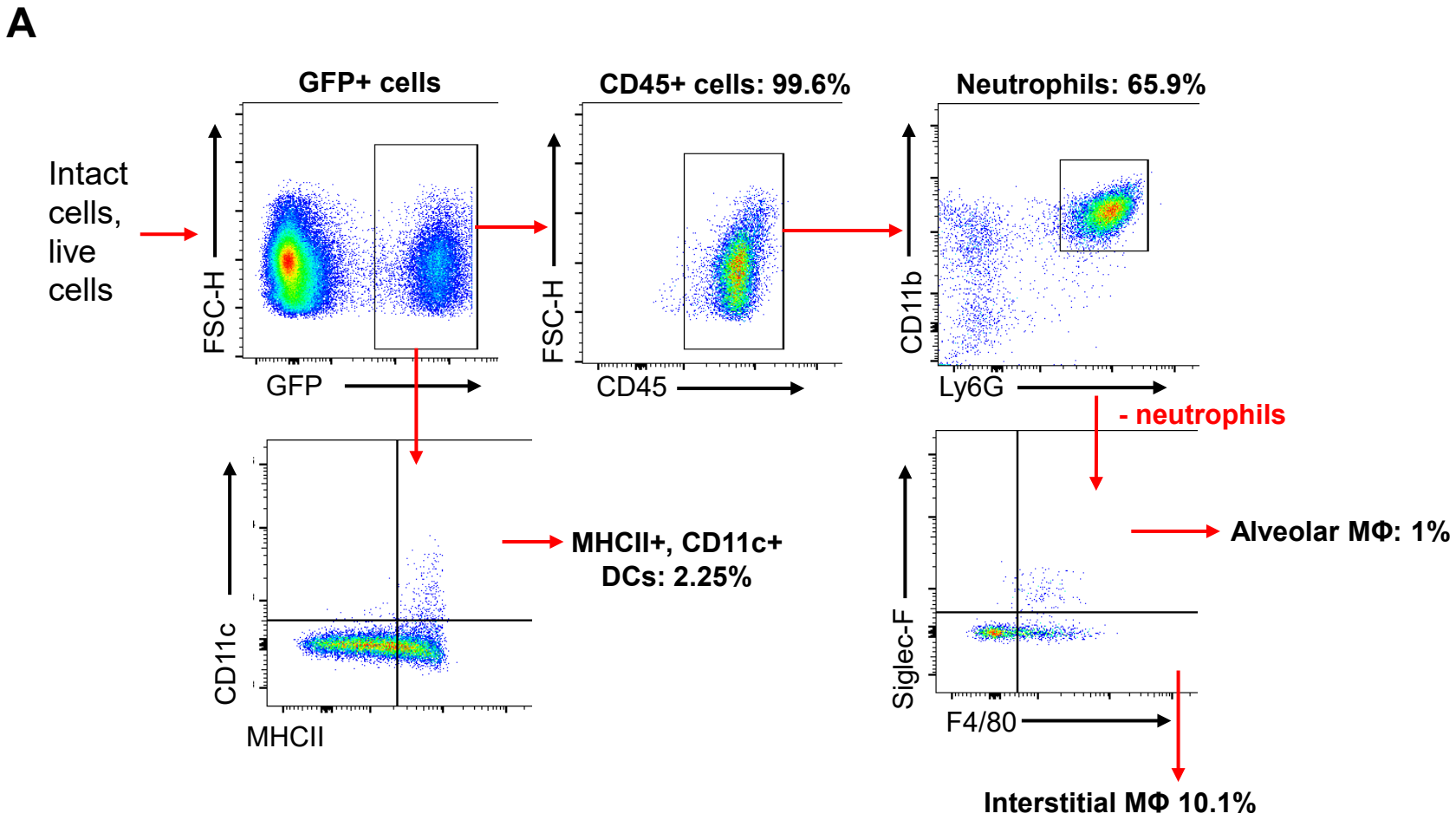
A
Intact cells, live cells
GFP+ cells
FSC-H
GFP
CD45+ cells: 99.6%
FSC-H
CD45
Neutrophils: 65.9%
CD11b
Ly6G
- neutrophils
MHCII+, CD11c+
DCs: 2.25%
CD11c
MHCII
Alveolar MΦ: 1%
Siglec-F
F4/80
Interstitial MΦ 10.1%

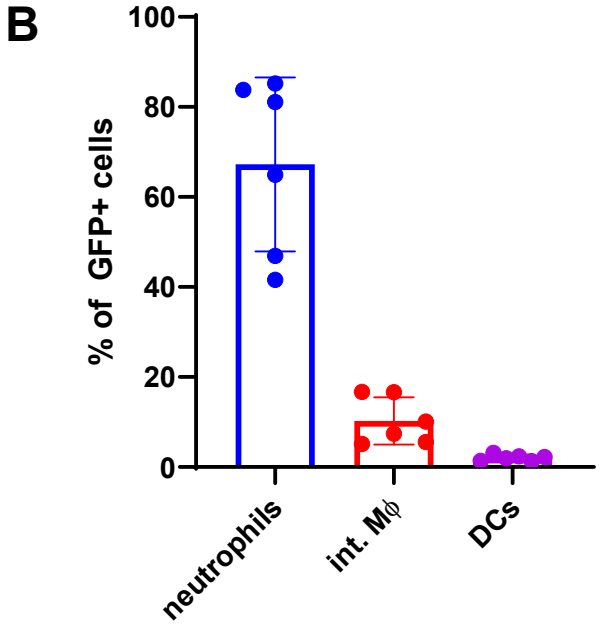
B
% of GFP+ cells
100
80
60
40
20
0
neutrophils
int. Mϕ
DCs

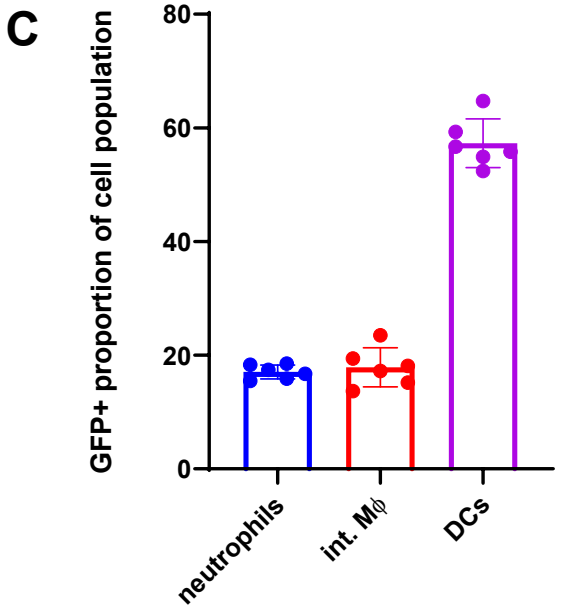
C
GFP+ proportion of cell population
80
60
40
20
0
neutrophils
int. Mϕ
DCs

D

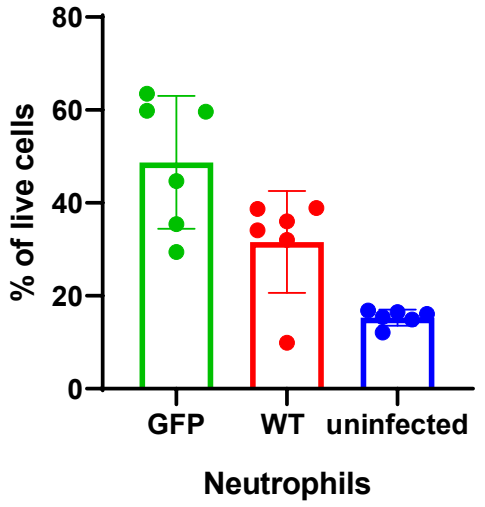
80
60
40
20
0
% of live cells
GFP
WT
uninfected
Neutrophils

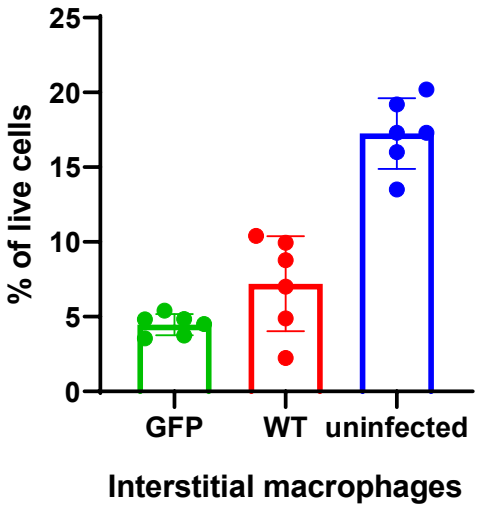
25
20
15
10
5
0
% of live cells
GFP
WT
uninfected
Interstitial macrophages

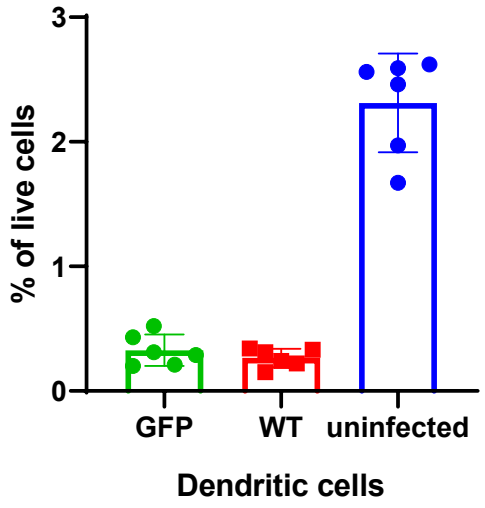
3
2
1
0
% of live cells
GFP
WT
uninfected
Dendritic cells

Figure 3: Identification of myeloid cell types associated with GFP-expressing E. africanus in mouse lung at 7 days post-infection. Scatter plots showing the strategy of gating on GFP first (A), which was used to identify myeloid cell types in the mouse lung that were GFP-positive (associated with the GFP reporter yeast), as summarised in (B). (C) Alternate gating on the various cell types first determined the proportions of each cell type associated with GFP yeast. (D) Myeloid cell distribution in the WT-and and GFP strain-infected mouse lung and in uninfected mouse lung. Differences in cell recruitment between WT- and GFP-strain-infected mice were not significant, $P>0.05$ (mean ± SD). n=6 mice per group, data is representative of two independent experiments.

A

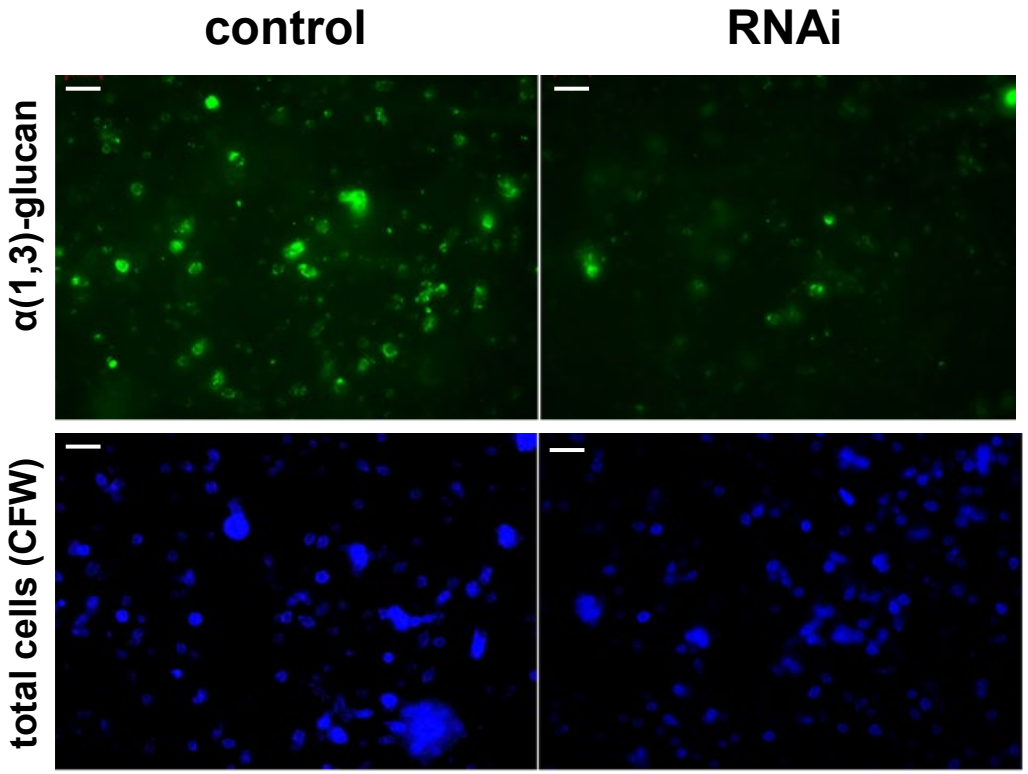
control
RNAi
α(1,3)-glucan
total cells (CFW)

B

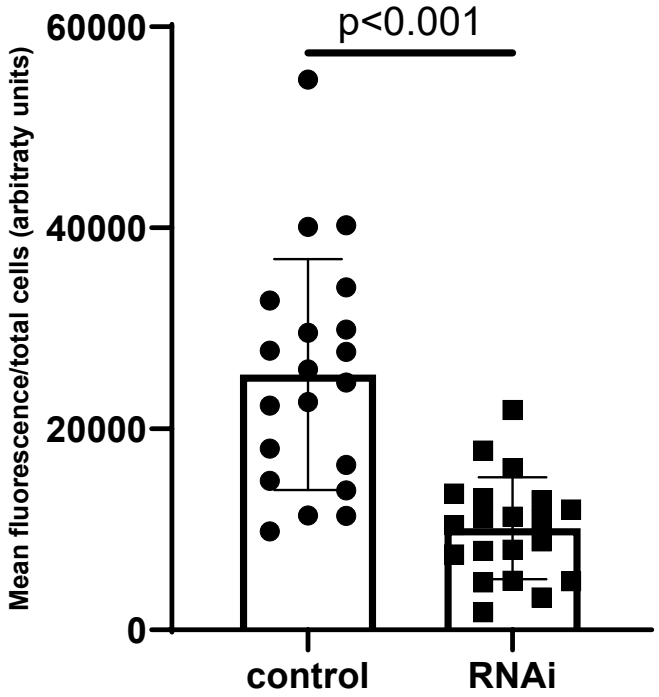
p<0.001
60000
40000
20000
0
Mean fluorescence/total cells (arbitraty units)
control
RNAi

Figure 4: (A) Cell wall staining and fluorescence microscopy of wild-type and AGS1 RNAi strains of E. africanus. E. africanus harbouring the AGS1 RNAi plasmid or the control GFP RNAi plasmid were stained with a monoclonal antibody specific for α(1,3)-glucan and calcofluor white (CFW) and examined by fluorescence microscopy. Imaging settings were kept constant for all samples. Bar=10μm (B) Background-corrected mean fluorescence intensity of microscopy images was measured and normalised by the number of cells per image. Ten images each from two independent experiments were analysed, Student's unpaired t-test, $p<0.001$.

A

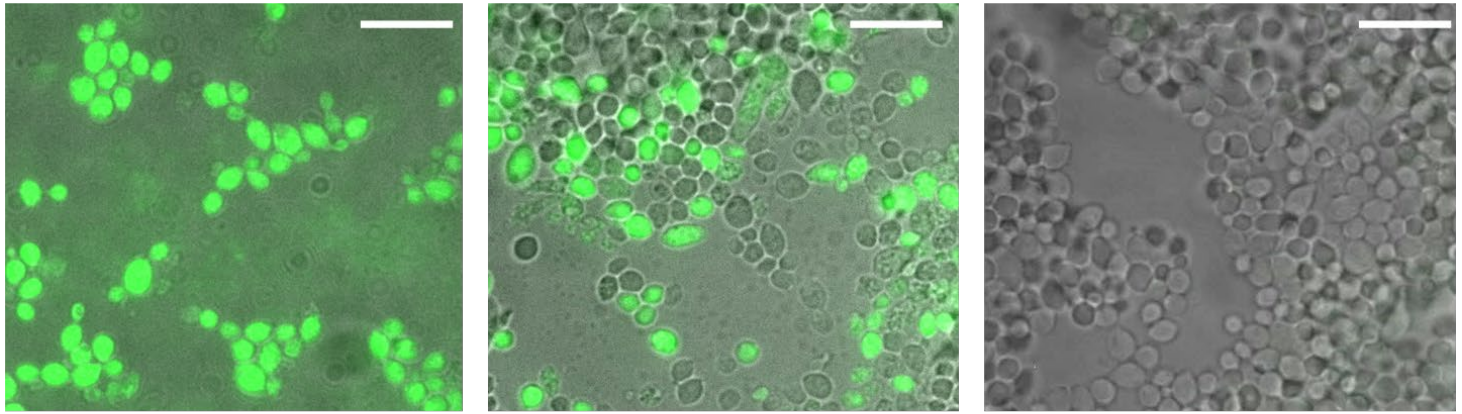

B

Sequencing: GFP-F

expected Cas9 cut site

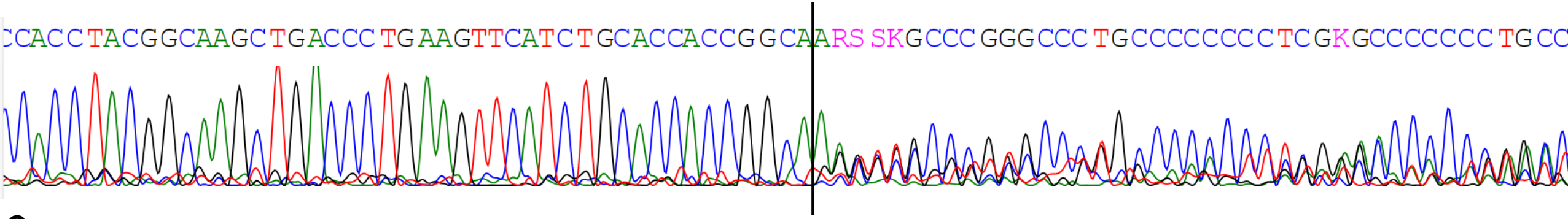

C

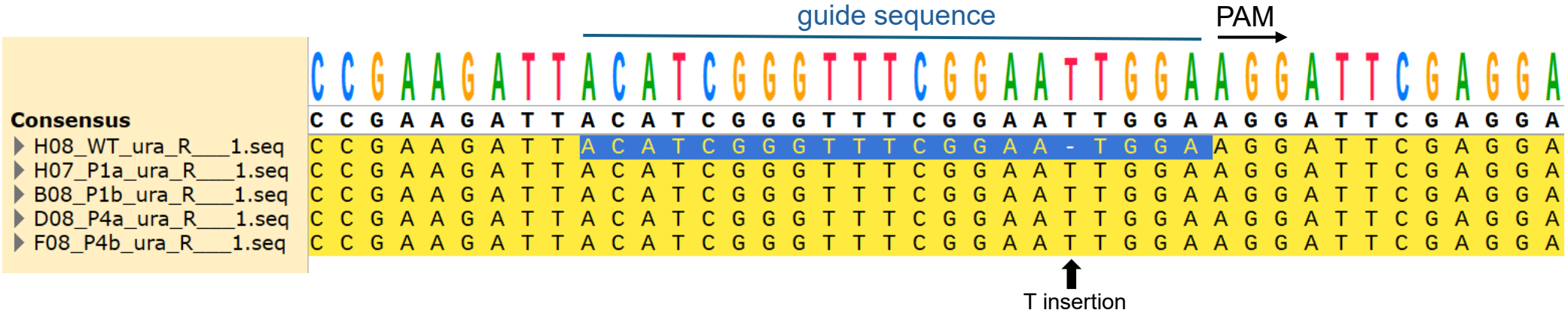

Figure 5: Evaluation of a CRISPR/Cas9 episomal system in E. africanus. (A) Merged fluorescence microscopy and brightfield images showing a decline in the proportion of fluorescent yeast cells with subsequent passages following transformation of GFP-expressing E. africanus with the CRISPR/Cas9 plasmid pSL01-sgGFP. Bar=10µm. (B) Sanger sequencing of a mixed population showed a mixture of signals following the expected Cas9 cut site, indicating the presence of various indels in the population. (C) Sequencing data of individually selected clones, aligned with the WT strain, following CRISPR/Cas9-mediated gene disruption of URA5. A T-insertion was observed in all clones.